Astrocytic HDAC7 Activates IKK/NF-κB Signaling to Regulate Neuroinflammation and Anxiety-like Disorders

Jinwang Ye
Shenzhen University
Suyue Zhong
Shenzhen University
Yunsong Deng
Shenzhen University
Xuanbao Yao
Shenzhen University
Qiong Liu
Shenzhen University
Jian-Zhi Wang
Huazhong University of Science and Technology
Shifeng Xiao (sxiao@szu.edu.cn)
Shenzhen University https://orcid.org/0000-0002-4753-6756

Research Article

Keywords: HDAC7, IKK, NF-κB, astrocyte, neuroinflammation, anxiety

Posted Date: March 24th, 2022

DOI: https://doi.org/10.21203/rs.3.rs-1462010/v1

Abstract

Class IIa histone deacetylase s (HDAC) have been shown to drive innate immune cell-mediated inflammation in the peripheral system, but their roles in cerebral inflammatory responses remain largely unknown. Here, we elucidate that HDAC7 is selectively elevated in lipopolysaccharide (LPS)-challenged astrocytes both in vivo and in vitro. We identify that HDAC7 binds to the inhibitory kappa B kinase (IKK) to promote IKKα and IKKβ deacetylation and subsequent activation, leading to the activation of nuclear factor κB (NF-κB). Astrocyte-specific overexpression of HDAC7 results in NF-κB activation, pro-inflammatory gene upregulation and anxiety-like behaviors in mice, while downregulating HDAC7 reserves LPS-induced NF-κB activation and inflammatory responses. Furthermore, pharmacological inhibition of HDAC7 by a class IIa HDAC inhibitor attenuates LPS-induced NF-κB activation, neuroinflammation and anxiety-like disorders both in vivo and in vitro. Together, our data reveal a novel mechanism of HDAC7 in astroglial inflammation and suggest that targeting HDAC7 could be a potential therapeutic strategy for the treatment of anxiety and other neuroinflammation-related diseases.

Introduction

Anxiety is a mental health disease characterized with excessive fear, anxiety and avoidance of perceived threats in internal to oneself or the environment. Considering the ongoing COVID-19 pandemic that has resulted in quarantine and social isolation, the rise in individuals suffering from anxiety has been particularly noticeable. Accumulating evidence suggest a tight link between neuroinflammation and the pathology in anxiety and other psychiatric disorders [1, 2]. Astrocytes are the most abundant glial cells and their dysfunction and activation have attracted increasing attention in the study of anxiety [3]. In the central amygdala, oxytocin-expressing astrocytes mediate neuronal activity and anxiolytic and positive reinforcement effects [4]. In the basolateral amygdala, lipopolysaccharide (LPS)-induced neuroinflammation contributes to anxiety and depressive-like behavior [5]. Moreover, inhibition of astrocytic inflammation has been evidenced to show beneficial effects on anxiety-like disorders [6, 7]. However, the underlying mechanisms of astrocyte-mediated neuroinflammation remain unclear.

The histone deacetylase (HDAC) family has been implicated in inflammatory process and anti-inflammatory effects of HDAC inhibitors have been recognized [8]. However, clinical trials have raised the potential of undesirable effects occurring upon pan-HDAC inhibitor treatment [9, 10]. Thus, investigation of selective HDAC might bring new insights in improving the therapeutic efficacy. In particular, the class IIa HDACs (HDAC4, 5, 7 and 9) are distinct from other HDACs as they rarely associate with histone tails [11] and can shuttle between the cytoplasm and nucleus to regulate signaling transduction and gene expression [12]. In the peripheral immune system, class IIa HDACs are shown to modulate immune response and drive innate immune cell-mediated inflammation [13, 14]. For instances, in a macrophage-dependent autochthonous breast cancer mouse model, application of a selective class IIa HDAC inhibitor, TMP195, can induce the recruitment and differentiation of highly phagocytic and stimulatory macrophages within tumors [15]. Myeloid-specific overexpression of HDAC7 amplifies LPS-induced inflammatory signature, while pharmacological or genetic inhibition of HDAC7 attenuates LPS-inducible

inflammatory responses [13]. Treatment of Class IIa inhibitor confers beneficial effects in LPS-induced acute kidney injury mice model as well [16]. However, the function of class IIa HDACs in the cerebral inflammation has been largely unexplored.

Nuclear factor κB (NF-κB), a pro-inflammatory transcriptional factor, is a key regulator of inflammation in central nervous system [17]. Under physical conditions, NF-κB is sequestered in the cytoplasm by the inhibitor of κB (IκB). In the canonical NF-κB activation pathway, signal-induced IκB phosphorylation by inhibitor of κB kinase (IKK) promotes IκB ubiquitination and subsequent degradation, leading to the release and nuclear translocation of NF-κB [18, 19]. IKK is composed of three subunits including two homologous catalytic subunits IKKα and IKKβ and a regulatory subunit IKKγ [20]. Recent studies have established a close link between class IIa HDACs and IKK/NF-κB signaling. For instance, HDAC4-knockout macrophages display increased NF-κB activity and proinflammatory genes expression with enhanced NF-κB acetylation [21]. Moreover, HDAC4 can directly SUMOylate IκBα and prevent its polyubiquitination and degradation, resulting in the inhibition of NF-κB [22]. HDAC9 can binds to IKKα and IKKβ, causing their deacetylation and subsequent activation, which drive NF-κB activation in both macrophages and endothelial cells [23]. These studies revealed the critical and intricate role of class IIa HDACs in modulating NF-κB activity in different cells and tissue organ types. However, their involvements in the brain remain unclear.

Here, we exhibit that LPS stimulation specifically increases the mRNA and protein expression levels of HDAC7 in astrocytes both in vivo and in vitro, with other class IIa HDACs nearly unchanged. Astrocyte-specific overexpression of HDAC7 in hippocampal CA1 promotes NF-κB activation, astrocyte activation and pro-inflammatory gene expression. Mechanically, HDAC7 binds to IKKα, IKKβ and IKKγ, resulting in IKKα and IKKβ deacetylation and activation, which promotes NF-κB nuclear localization. Pharmacological inhibition or knockdown of HDAC7 rescues LPS-induced NF-κB activation, neuroinflammation and anxiety-like disorders. Together, our results demonstrate a critical role of astrocytic HDAC7/IKK/NF-κB signaling in LPS-induced neuroinflammation and anxiety.

Materials And Methods

Animals

Adult male C57BL/6 mice (two month old) were purchased from Changzhou Cavens Laboratory Animal Co., Ltd. The mice were housed in groups of four to five per cage with ad libitum access to food and water, and were maintained under a 12-h light/dark cycle (lights on at 7:00 p.m., off at 7:00 a.m.) at a stable temperature (22 ± 2°C). In the present study, we have complied with all relevant ethical regulations for the animal testing and research. All procedures were approved by institutional guidelines and the Animal Care and Use Committee (Shenzhen University, Shenzhen, China) of the university’s animal core facility.

Behavioral tests

Open field test (OFT)

The OFT is used to measure the anxiety-like behavior in mice. The OFT apparatus is made of transparent plastic (50 cm × 50 cm× 40 cm, length × width × height) and the central zone area was defined as 50% of the open field arena. Each mouse was brought to the room and acclimated for at least 1 hour before the behavioral test. Individual mouse from each group was placed in the center area of the arena and permitted for free exploration. Their activity was videotaped from the top of the arenas for 10 min by a video camera. The time spent in the center area, the number of central area crossings, and center moving distance were recorded by video-tracking and behavioral analysis software (SMART v3.0 software).

Elevated plus maze (EPM)

EPM was performed to evaluate the anxiety-like behavior in mice. The EPM apparatus consists of two opposing open arms (66 cm × 6 cm) and two opposing closed arms (66 cm × 6 cm) intersecting at 90 degrees in the form of a plus, with a central area (6 cm × 6 cm). The EPM was elevated 50 cm above the floor in a dim and quiet room without any human disturbance during the test. Mouse from each group was placed in the center area and allowed to explore the EPM for 10 min freely. The time spent in open arms, the total number of entries into the open arm and total distance in open arms were recorded by video-tracking and behavioral analysis software (SMART v3.0 software). Between each trial, the maze was cleaned with 75% ethanol.

Cell culture

For primary mouse astrocyte culture, astrocytes were isolated from 12-24 hours neonatal C57BL/6 mice. The cortex was isolated and minced into ice-cold Hank's buffered saline solution, and incubated in 0.25% trypsin at 37 °C for 15 min. Then the tissue was gently triturated eight to ten times to dissociate the cells and obtain a homogenous cell suspension. The density of cells was determined by a hemocytometer. Astrocytes were planted with the DMEM-high glucose medium containing 10% FBS onto poly-D-lysine-precoated flasks. After 5-7 days, when the cell density reached 75%-90%, the astrocytes were sorted at shake cultivation rotating at 200-220 r/min overnight. Then the medium was discarded and the cells were incubated with DMEM containing 0.25% trypsin for 5 min, and centrifuged at 1000 g for 5 min after addition of the culture medium. After resuspension, cells were plated onto culture plate with 5×10^5 per well for western blotting and RT-qPCR analysis and 1×10^5 per well for cell imaging. The culture medium was changed every 3 days throughout the cultivation process.

HEK293 WT cells were cultured with 90% DMEM-high glucose medium and 10% fetal bovine serum (FBS), 100 U/ml penicillin, 0.1 mg/ml streptomycin (all from Hyclone) at 37 °C in the presence of 5% CO_2. Transfection was performed with Neofect (Neofect biological Technology, Beijing) when cells were cultured to 70%~80% confluence in six-well plates. 48 hours after transfection, cells were collected and lysed for further research.

Western blotting and Co-immunoprecipitation

Mice hippocampal CA1 were carefully separated using a microtome in ice-cold PBS, then homogenized in RIPA buffer containing 1mM PMSF and 0.1% cocktail. Cultured cells were washed with ice-cold PBS twice and homogenized in RIPA buffer as described. After centrifugation at 10000 *g* for 15 min, the supernatant was extracted and protein concentration test was taken up, the loading buffer (50Mm Tris-HCL, 2% SDS, 10% glycerol, pH 7.6) was added in the homogenates and samples were boiled at 95 ℃ for 10 min. The protein samples were separated by SDS/PAGE and transferred onto nitrocellulose membranes (Whatman), then incubated with primary antibodies at 4 ℃ overnight. Secondary antibodies incubation was performed at room temperature for 1 h. Immunoreactive bands were visualized with an electroluminescence kit and scanned for densitometric analysis using an imaging system (Image Station 4000 M; Kodak).

For co-immunoprecipitation, cells after treatment were homogenized in RIPA buffer containing 1mm PMSF and 0.1% cocktail, then centrifuged at 12,000 *g* for 10 min. The supernatant was incubated with primary antibodies at 4 ℃ for 6 hours followed by a 2-hour incubation with protein A + G agarose. The resins were washed three times with PBS, resuspended with 2 × loading buffer and boiled at 95 ℃ for 10 min. Immuno-precipitates were analyzed by western blotting.

RT-qPCR

Mice brain tissues were dissected and immediately frozen in liquid nitrogen. Cultured cells were quickly collected and incubated with ice-cold TRIzol (No. 15596026, Invitrogen, USA) after the medium removal. Total RNA isolation from mice brains and cultured cells were performed following the manufacturer's protocol. The RNA concentration and purity were measured using a NanoDrop 2000 spectrophotometer (Thermo Scientific, USA). The RNA-to-cDNA reverse transcription reaction was carried out using a Prime Script RT Kit (RR047A, Takara, Japan). Briefly, right before reverse transcription reaction, the genomic DNA removing reaction was performed at room temperature for 30 min, and then the reaction mixture was added to the RNA solution, and the RNA/reagent mixture was incubated at 37 °C for 15 min, further heated at 85 °C for 5 sec, and cooled to 4 °C. RT-qPCR was performed using SYBR Master Mix on a Bio-Rad Connect Real-Time PCR platform (Bio-Rad, USA). The reaction was carried out in a DNA thermal cycler under the following conditions: 95 °C for 30 s, 39 cycles of 95 °C for 5 s and 60 °C for 30 s, 72 °C for 30 s, and 95 °C for 15 s, 60 °C for 30 s, 95 °C for 5 s and 4 °C for 60 s. The resulting Cq values were calculated (using the $2^{-\Delta\Delta CT}$ method) and β-actin was used as a housekeeping gene. The RT-qPCR primer sequences are listed in Table 1.

Immunofluorescence

Cultured cells were fixed in 4% (vol/vol) paraformaldehyde for 15 min and permeabilized in phosphate buffer containing 0.5% triton X-100. Non-specific binding was blocked by PBST buffer containing 3% BSA for 1 h. Primary antibodies were incubated at 4 ℃ overnight. The secondary antibodies conjugated to Alexa-Fluor 488/546 were added to the coverslip for 1 h at 37 ℃, followed by Hoechst staining for 10

min. The coverslips were washed and mounted onto slides. All the images were observed with the LSM880 confocal microscope (Zeiss, Germany).

Viruses, Reagents and Antibodies

The IKKα-HA, IKKβ-HA, IKKγ-HA, IκBα-HA and EGFP-HDAC7 plasmids were constructed in the pcDNA3.1 vector. The HDAC7 overexpression lentivirus lenti-GfaABC1D-HDAC7-P2A-eGFP, HDAC7 knockdown lentivirus lenti-GfaABC1D-shHDAC7-eGFP(mir30), AAV-GfaABC1D-HDAC7-eGFP and corresponding controls were constructed and packaged by Obio Technology (Shanghai, China), and the target sequences of HDAC7 are TGCGCTACAAACCCAAGAAAT and CCATGTTTCTGCCAAATGTTT. Lentiviruses were used in primary astrocytes with Multiplicity of infection (MOI) of 10. AAV2/8 was used in mice experiments.

Lipopolysaccharide (LPS) from Escherichia coli, strain 055: B5 was purchased from Absin (Shanghai, China). TMP195 (a selective class IIa HDAC inhibitor) was purchased from Selleck (Shanghai, China). All other reagents were from Sigma-Aldrich (USA).

IKKα (1:500 for WB, 2682), IKKβ (1:500 for WB, 2678), IKKγ (1:500 for WB, 2695), IKBα (1:500 for WB, 4814), Iba1 (1:50 for IF, 36618), NF-κB (1:500 for WB, 1:100 for IF, 1:100 for IP, 8242), p-NF-κB-Ser468 (1:500 for WB, 3039), p-NF-κB-Ser536 (1:500 for WB, 3033), HA Tag (1:500 for WB, 1:100 for IP, 3724), Acetylated-Lysine (1:1000 for WB, 9441), IgG (1:100 for IP, 2729), GFAP (1:1000 for WB, 1:200 for IF, 36707), INOS (1:500 for WB, 1:100 for IF, 13120), Il1α (1:500 for WB, 50794), P38 (1:1000 for WB, 8690), p-P38 (1:1000 for WB, 4511), ERK1/2 (1:1000 for WB, 4695) and p-ERK1/2 (1:500 for WB, 4370) were from Cell Signaling. HDAC4 (1:1000 for WB, 07-1490), HDAC7 (1:1000 for WB, 1:100 for IF, 1:100 for IP, H2662) were from Thermo Scientific. HDAC5 (1:1000 for WB, ab55403), HDAC9 (1:1000 for WB, ab109446), NeuN (1:200 for IF, ab104224), LaminB1 (1:1000 for WB, ab16048), COX-2 (1:500 for WB, ab179800) and beta-actin (1:1000 for WB, ab6272) were from Abcam. Iba1 (1:200 for IF, 012-26723) was from Wako.

Statistical analysis

Data are expressed as mean ± SEM and analyzed using the GraphPad Prism 8 statistical software. The one-way or two-way ANOVA was used to determine the differences among four groups and the Student's t test was used for two groups. The significance was assessed at $p < 0.05$.

Results

1. HDAC7 levels are increased in LPS-stimulated astrocytes in vivo and in vitro

Class IIa HDAC drives innate immune response in the peripheral immune system. To explore the involvement of IIa HDACs in neuroinflammation in the brain, 2-month-old male C57BL/6 mice were intraperitoneally injected with LPS (3 mg/kg) or normal saline and sacrificed 24 hours after injection. Interestingly, through RT-qPCR tests, we found that LPS-treatment dramatically increased HDAC7 mRNA

levels both in the hippocampus and cortex (Fig. 1A and 1B), with a slightly reduction of HDAC9 in the cortex and other HDACs unchanged (Fig. 1B). Further studies confirmed uniquely upregulated HDAC7 protein levels both in the hippocampus (Fig. 1C and 1E) and cortex (Fig. 1D and 1F) as well. Strikingly, co-immunostaining showed that elevated HDAC7 was mostly located in activated astrocytes in LPS-injected mouse brain (Fig. 1G), while neuronal HDAC7 remained unaffected (Fig. 1H). HDAC7 expression in microglia was relatively low and little difference was seen after LPS treatment (Fig. 1I). To further identify the role of IIa HDACs in astrocytes, primary cultured astrocytes were treated with LPS (100 ng/ml) for 24 hours. Consistent with the results observed in vivo, LPS-treatment markedly increased HDAC7 mRNA level (Fig. 1J) and protein expression protein (Fig. 1K and 1L) and in cultured astrocytes. LPS-induced HDAC7 upregulation was detected mainly in the cytoplasm as shown by immunofluorescence staining (Fig. 1M). These in vivo and in vitro data suggest that HDAC7 may play a unique role in LPS-induced astrocyte activation and neuroinflammation.

2. Astrocyte-specific overexpression of HDAC7 leads to neuroinflammation and anxiety-like behaviors in mice

To verify the role of astrocytic HDAC7 in neuroinflammation in vivo, we specially overexpressed HDAC7 in astrocytes by stereotaxically injecting AAV-GfaABC1D-HDAC7-eGFP or AAV-GfaABC1D-eGFP into the dorsal hippocampal CA1 subset of 2-mon-old wildtype male C57BL/6 mice. The expression of AAV-GfaABC1D-HDAC7-eGFP in astrocytes was confirmed by immunofluorescence imaging at one month after injection (Fig. 2A). Overexpression of HDAC7 induces distinct astrocyte activation, as shown by hypertrophic morphology and enhanced glial fibrillary acidic protein (GFAP) expression (Fig. 2A. 2C and 2D). RT-qPCR analysis of Il-1α, Il-1β, Il6, tumor necrosis factor α (Tnfα), Gfap and complement C3 (C3) revealed remarkable pro-inflammatory responses in HDAC7-overexpressing mice (Fig. 2B). In light of the central role of NF-κB in astrocyte-mediated neuroinflammation and the resemblance of HDAC7-related inflammatory gene expression with NF-κB-driven transcriptional responses, we hypothesized that NF-κB might be a downstream effector of HDAC7. As suggested, western blotting analysis showed that astrocytic overexpression of HDAC7 increased NF-κB phosphorylation levels at Ser468 and Ser536 normalized to total NF-κB (Fig. 2C, 2E and 2F). Immunofluorescence staining also identified enhanced nuclear localization of NF-κB in HDAC7-overexpressing astrocytes compared to GFP-expressing astrocytes (Fig. 2G). These data implicate that NF-κB could act as a downstream effector of HDAC7.

Given the prominent inflammatory response in HDAC7-overexpressing mice, the effects of HDAC7 on psychiatric and cognitive behaviors were measured. We observed obvious anxiety-like behaviors in HDAC7-overexpressing mice, evidenced by reduced center distance (Fig. 2I), center exploring time (Fig. 2J) and center entries (Fig. 2K) in the open field test (OFT) and decreased travel distance (Fig. 2M), spending time (Fig. 2N) and entries (Fig. 2O) in the open arm in elevated plus maze (EPM) test. Interestingly, HDAC7-overexpressing mice performed normally as the controls in the Morris water maze (data not shown). Thus, we concluded that astrocytic overexpression of HDAC7 promotes neuroinflammation and anxiety-like disorders involving NF-κB signaling.

3. HDAC7 activates IKK through binding to and deacetylating IKKα and IKKβ.

To gain mechanistic insights in HDAC7 and NF-κB activation, coimmunoprecipitation experiments were carried out by co-transfection of HDAC7 and IKKα, IKKβ, IKKγ or IκBα respectively in HEK293 cells. HDAC7 was shown to bind to IKKα, IKKβ and IKKγ, but not IκBα (Fig. 3A, 3D, 3G and 3J). Of note, we observed increased protein levels of HA-tagged IKKα, IKKβ and IκBα with reduced HA-tagged IKKγ level (Fig. 3A, 3B, 3D, 3E, 3G, 3H, 3J and 3K). To explore the underlying consequence of HDAC7-IKK interactions, we determined the acetylation status of IKKα, IKKβ and IKKγ. The acetylation of IKKα and IKKβ were reduced in HDAC7-overexpressing cells (Fig. 3A, 3C, 3D and 3F), while IKKγ acetylation level kept unvaried (Fig. 3G and 3I). IKK deacetylation is believed to enhance their activity. Thus, we tested IKKβ activity and found increased IKKβ activity as evidenced by increased phosphorylation levels of NF-κB P65 at Ser468 and Ser536 in an immunoprecipitation-based kinase activity assay (Fig. 3L-O). To further extend our findings in astrocytes, we overexpressed HDAC7 in primary cultured mouse astrocytes via infection of lenti-GfaABC1D-HDAC7-GFP or lenti-GfaABC1D-GFP. We found increased nuclear NF-κB level and unaffected cytoplasm NF-κB level upon HDAC7 overexpression (Fig. 3P and 3Q). In contrast, little effect of HDAC7 on p38 mitogen-activated protein kinase (MAPK) and extracellular signal-regulated protein kinases 1/2 (ERK1/2) signaling was detected (Supplementary Fig. 1), further corroborating the specificity of the downstream signaling events induced by HDAC7/IKK interactions. Together, these findings identified IKK/NF-κB signaling as a key downstream effector linking HDAC7 to astrocytic inflammation.

4. Inhibition of HDAC7 attenuates LPS-induced NF-κB activation and inflammatory responses in cultured astrocytes.

To identify whether knockdown of HDAC7 can rescue NF-κB activation and inflammation responses in astrocytes, we downregulated HDAC7 in cultured mouse astrocytes through infection of lenti-GfaABC1D-shHDAC7-eGFP-WPRE(miR30) or control lenti-GfaABC1D-eGFP-WPRE(miR30) for 5 days, and then treated cells with LPS (100 ng/ml) for 24 hours. We found that knockdown of HDAC7 efficiently inhibited LPS-induced NF-κB phosphorylation at Ser468 and Ser536 (Fig. 4A-C). Moreover, upon LPS stimulation, the protein levels of IKKα and IKKβ were comparable in GFP control and HDAC7 knockdown cells (Fig. 4D-F), while IKKγ was slightly increased by downregulating HDAC7 (Fig. 4D and 4G). In addition, HDAC7 knockdown cells showed augmented IκBα protein level compared to GFP cells in LPS-treated group (Fig. 4D and 4H). We also found that HDAC7 knockdown attenuated LPS-induced pro-inflammatory gene expression, as shown by markedly reduced mRNA levels of Il-1α, Il-1β, Il6, Tnfα, cyclooxygenase-2 (COX-2) and inducible nitric oxide synthase (iNOS) (Fig. 4I). Furthermore, LPS-induced protein expressions of Ptgs2, INOS and Il-1α were also abolished in HDAC7 knockdown cells (Fig. 4J-M).

Previous studies have reported that TMP195, a selective class IIa HDAC inhibitor with high affinity of HDAC7, may have potential in attenuating inflammatory response [16, 23]. Thus, we studied the effect of TMP195 in the mouse primary astrocytes by pretreating the cells with TMP195 (3/5 μM) for 1 hour, and then with the mixture of LPS (100 ng/ml) and TMP195 (3/5 μM) for 24 hours. Consistent with the results of genetically HDAC7 knockdown, TMP195 treatment dose-dependently blocked LPS-induced NF-κB

phosphorylation at Ser468 and Ser536 (Fig. 5A-C), and attenuated the LPS-induced NF-κB nuclear translocation (Fig. 5D). Correspondingly, the reduced mRNA levels of NF-κB-targeted pro-inflammatory molecules Il-1α, Il-1β, Il6, Tnfα, COX-2 and iNOS were confirmed in TMP195-treated cells by RT-qPCR analysis (Fig. 5E). Further western blotting analysis of iNOS, COX-2 and Il-1α also verified the anti-inflammatory effects of TMP195 (Fig. 5F-I). Collectively, these results identified HDAC7 as a pivotal driver of IKK/NF-κB pathway in LPS-induced neuroinflammation.

5. Pharmacological HDAC7 inhibition attenuates neuroinflammation, gliosis and anxiety-like disorders in vivo

Given the anti-inflammatory effects of TMP195 in vitro, we examined the therapeutic implication of TMP195 in vivo. 2-mon-old male C57BL/6 mice were intraperitoneally pre-injected with TMP195 (30/50mg/kg) 2 hours before injection of LPS or control saline (3 mg/kg, intraperitoneal injection), and followed by a second injection of TMP195 (30/50 mg/kg, intraperitoneal injection) 6 hours after LPS treatment (Fig. 6A). Consistent with the in vitro findings, western blotting showed that TMP195 treatment ameliorated LPS-induced NF-KB phosphorylation at Ser468 and Ser536 in the hippocampus (Fig. 6B-D) and cortex (Fig. 6F-H), along with decreased GFAP expression (Fig. 6E and 6I). RT-qPCR analysis of Il-1α, Il-1β, Tnfα, Gfap, C3 and lipocalin-2 (Lcn2) also revealed a comprehensively reduced inflammatory responses in TMP195-treated mouse hippocampus (Fig. 6J) and cortex (Fig. 6K). Simultaneously, LPS-induced astrocytes and microglia activation in the hippocampus was also attenuated as demonstrated by mitigated GFAP and Iba1 expression and preserved resting morphology (Fig. 7A and 7B). Together, these results suggest that pharmacological inhibition with TMP195 attenuates LPS-induced NF-KB activation and inflammatory responses in vivo.

Given that astrocytic overexpression of HDAC7 induces anxiety-like disorders, we thus evaluated the therapeutic effects of TMP195 treatment on anxiety via the open field test and elevated plus maze test (Fig. 7C). In the OFT, treatment with high concentration (50 mg/kg) of TMP195 arrested LPS-induced behavioral disorders, as shown by restored moving distance (Fig. 7D), exploring time (Fig. 7E) and zone entries (Fig. 7F) in the center region, while low concentration (30 mg/kg) of TMP195 exhibited no significant therapeutic effects. In the elevated plus maze test, both low and high concentrations (30/50 mg/kg) of TMP195 treatment efficiently rescued LPS-induced anxiety-like behaviors (Fig. 7G), as demonstrated by increased travel distance (Fig. 7H), spending time (Fig. 7I), and entries (Fig. 7J) in the open arm. Notably, the rescue effect of TMP195 exhibited a dose-dependent manifestation. Collectively, these results demonstrate that therapeutic HDAC7 inhibition with TMP195 prevents LPS-induced neuroinflammation, gliosis and anxiety-like disorder.

Discussion

In the present study, we demonstrate that astroglial HDAC7 is a key regulator of LPS-induced neuroinflammatory responses and anxiety-like disorders. Among the four IIa HDACs, HDAC7 is selectively elevated in LPS-challenged astrocytes both in vivo and in vitro. We have shown that HDAC7 directly

deacetylates IKKα and IKKβ to enhance IKK activity, resulting in NF-κB activation, inflammatory gene expression and anxiety. Moreover, genetic or pharmacological inhibition of HDAC7 can effectively prevent LPS-induced NF-κB activation, neuroinflammation and anxiety-like disorders both in vivo and in vitro, supporting a potential anti-inflammatory therapeutic strategy of targeting HDAC7.

Glia cells activation and neuroinflammation are the leading cause of LPS-induce anxiety-like behaviors in mice. Our data showed that pharmacological inhibition of HDAC7 with TMP195 rescued LPS-induced anxiety-like disorders, as demonstrated by restored distance, time and entries in the center zone in the open filed test and increased mobility to exploring the open arm in the elevated plus maze test in TMP195-treated mice compared to vehicle-treated mice. These beneficial effects could be attributed to TMP195-attenuated inflammatory responses, as shown by reduced mRNA levels of Il-1α, Il-1β, Tnfα, Gfap, C3 and Lcn2. This is in accordance with previous studies that described the beneficial effects on anxiety-like disorders by blocking inflammation [1, 7]. In addition, neuroinflammation is a common hallmark pathology of multiple neurodegenerative diseases, such as Alzheimer's disease and Parkinson disease, our positive data on LPS-challenged models might bring new insights in these chronic inflammatory diseases.

HDAC inhibition was described as potent anti-inflammatory strategy in several immune-mediated diseases [8, 24]. In the present study, we focused on class IIa HDACs and found that HDAC7 level is selectively increased in astrocytes both in vivo and vitro upon LPS treatment. Further in vivo studies on astrocytes through delivery of AAV-GfaABC1D-HDAC7-eGFP into the hippocampal CA1 subset demonstrate an apparent astrogliosis and increased pro-inflammatory responses in HDAC7-overexpressing brain. Interestingly, similar increases in HDAC7 expression in inflammatory macrophages and enhanced inflammatory signature in myeloid-specific HDAC7 overexpressing macrophages upon LPS stimulation have been reported by *Sweet*'s group [13, 14]. Despite the consistent aspects between our study and that of *Sweet*'s group, there were noticeable differences. Specially, *Sweet*'s group reported increased inflammatory gene expression in HDAC7-overexpressing macrophages dependent on Toll-like Receptor 4 activation through LPS stimulation [13], whereas we observed enhanced inflammatory responses and astrogliosis independent of stimulation of exogenous antigens. This may be explained by the cell-type/tissue-restricted discrepancies or by the mechanic differences mediated by HDAC7 in macrophages and astrocytes. Indeed, we demonstrate here that HDAC7 activates IKK/NF-KB signaling to regulate astrocytic inflammation, different from the HDAC7-PKM2 signaling axis described by *Sweet*'s group.

NF-κB has been identified as a key transcriptional activator of astrocytic activation and neuroinflammation [25, 26]. Upon extracellular stimuli, IKK could be activated promptly, resulting in IKB phosphorylation and subsequent degradation by the proteasome, eventually promoting NF-κB nuclear translocation and pro-inflammatory gene transcription [20]. IKK activity is controlled by multiple posttranslational modifications, including phosphorylation and acetylation. Although a body of literature was generated on phosphorylation-mediated IKK activation and deactivation, the molecular regulating machinery involved in acetylation and deacetylation such as HDACs remained to be elucidated. In the

current study, we demonstrated that HDAC7 could deacetylate IKKα and IKKβ and thus strengthen IKK activity, evidenced by upregulated NF-κB phosphorylation and nuclear NF-κB level. Highly consistent with our results, a previous study reported that HDAC9, another member of class IIa HDACs, can activate IKK through deacetylation of IKKα and IKKβ and promote NF-κB signaling activation [23]. Moreover, upon LPS stimulation, we observed augmented IKBα expression in HDAC7-knockdown cells, which also suggest an impaired IKBα degradation and infer a reduced IKK activity by downregulating HDAC7. Anyway, a well-defined deacetylation site on IKKα and IKKβ mediated by HDAC7 remains unclear, more mass spectrometry analysis is needed in the future. The activating effects of HDACs in NF-κB signaling have also been reported in other HDAC families. For examples, NF-κB acetylation is increased in HDAC1/2 double knockout mice [27], HDAC3 directly interacts with NF-κB p65 and is involved in the removal of the inhibitory NF-κB p65 acetylation [28], inhibition of HDAC6 suppresses LPS-activated NF-κB signaling pathway in RAW264.7 macrophages [29]. Our exploration on HDAC7 provide new mechanic insights for NF-κB signaling study.

Previous reports in peripheral immune systems have provided evidence for the anti-inflammatory effect of targeting class IIa HDACs [13, 23]. By using TMP195, a selective class IIa HDAC inhibitor, in LPS-induced neuroinflammation models, we observed reduced neuroinflammation including Il1α, Il1β, Tnfα and C3, attenuated gliosis and reversed anxiety-like behaviors, implying that HDAC7 is a critical regulator of LPS-induced neuroinflammation. However, the involvement of other HDACs in the TMP195-treated studies cannot be rudely ruled out. Indeed, we declared here that HDAC7 has a dominant role, but multiple other class IIa HDACs could interact with IKK and contribute to inflammatory responses. For example, HDAC5 interact with IKKβ [30] and HDAC9 interact with both IKKα and IKKβ in HEK293 cells [23]. In vivo studies also demonstrate that knockdown of HDAC5 reduces LPS-induced inflammatory gene expression [31] and knockout of HDAC9 reduces vascular inflammation in a mouse model of atherosclerosis [23]. Thus, it is possible that HDAC5 and HDAC9 may be partly involved in therapeutic effects accompanied by TMP195. It is uncertain whether specific knockout of astrocytic HDAC7 in vivo has a protective function in neuroinflammation. The creation of mice with tissue-specific knockout of HDAC7 in astrocytes may address this issue. Of note, we also observed that TMP195 treatment reverses LPS-induced microglia activation. Microglia are resident immune cells in the brain and play a crucial role in neuroinflammation involving microglia-astrocyte crosstalk. The endogenous crosstalk between astrocytes and microglia regulates anti-inflammatory actions via the C3/C3aR signaling pathway. Previous studies have demonstrated that complement C3 released by NF-κB-activated astrocytes can modulate microglia immune homeostasis through C3a receptor expressed on microglia [32, 33], and knockout of C3 reduces microglia activation and proinflammatory cytokines levels [34, 35]. Indeed, we observed reduced C3 expression in both hippocampus and cortex of TMP195-treated mice compared with the control LPS-treated mice, providing a potential explanation for the blocking effects of TMP195 on microglia immune response.

To conclude, this study demonstrated a mechanistic explanation for the prominence of astrocytic HDAC7 in LPS-induced NF-κB activation and neuroinflammation and provided a novel therapeutic strategy of targeting HDAC7 for preventing neuroinflammation and anxiety.

Abbreviations

LPS: Lipopolysaccharide

HDAC:histone deacetylase

IKK: inhibitory kappa B kinase

NF-κB: nuclear factor κB

IκB:inhibitor of κB

COX-2:cyclooxygenase-2

iNOS: inducible nitric oxide synthase

GFAP: glial fibrillary acidic protein

C3: complement C3

Lcn2: lipocalin-2

Tnfa: tumor necrosis factor α

OFT: open field test

EPM: elevated plus maze

Declarations

Acknowledgements

The authors thank the Instrumental Analysis Center of Shenzhen University for technical assistance.

Finding

This work was financially supported by the Shenzhen Science and Technology Innovation Commission (JCYJ20180507182417779, JCYJ20200109110001818); the Natural Science the Foundation of China (82101493); and the China Postdoctoral Science Foundation (2021M692191).

Conflict of Interest

The authors declare no conflicts of interest in regards to this manuscript.

Author Contributions

Author contribution: Conceptualization, J.W.Y. and S.F.X.; Investigation, J.W.Y., S.Y.Z., Y.S.D. and X.B.Y.; Writing manuscript, J.W.Y. and S.F.X.; Funding Acquisition, J.W.Y. and S.F.X.; Resources, S.F.X., Q.L. and J.Z.W.; Supervision, S.F.X. and Q.L.

Data Availability

The datasets used or analyzed during the current study are available from the corresponding author on reasonable request.

Ethics approval

All animal experiments were approved by institutional guidelines and the Animal Care and Use Committee (Shenzhen University, Shenzhen, China) of the university's animal core facility.

Consent for Publication

Not applicable.

Consent to participate

Not applicable

References

1. Lama, A., et al., *Palmitoylethanolamide dampens neuroinflammation and anxiety-like behavior in obese mice.* Brain Behav Immun, 2022. **102**: p. 110-123.
2. Fang, Y., et al., *Fluoxetine inhibited the activation of A1 reactive astrocyte in a mouse model of major depressive disorder through astrocytic 5-HT2BR/beta-arrestin2 pathway.* J Neuroinflammation, 2022. **19**(1): p. 23.
3. Rossi, S., et al., *Neuroinflammation drives anxiety and depression in relapsing-remitting multiple sclerosis.* Neurology, 2017. **89**(13): p. 1338-1347.
4. Wahis, J., et al., *Astrocytes mediate the effect of oxytocin in the central amygdala on neuronal activity and affective states in rodents.* Nat Neurosci, 2021. **24**(4): p. 529-541.
5. Zheng, Z.H., et al., *Neuroinflammation induces anxiety- and depressive-like behavior by modulating neuronal plasticity in the basolateral amygdala.* Brain Behav Immun, 2021. **91**: p. 505-518.
6. Shim, H.S., et al., *Role of astrocytic GABAergic system on inflammatory cytokine-induced anxiety-like behavior.* Neuropharmacology, 2019. **160**: p. 107776.
7. Zhuang, X., et al., *IL-33 in the basolateral amygdala integrates neuroinflammation into anxiogenic circuits via modulating BDNF expression.* Brain Behav Immun, 2022. **102**: p. 98-109.
8. Shakespear, M.R., et al., *Histone deacetylases as regulators of inflammation and immunity.* Trends Immunol, 2011. **32**(7): p. 335-43.

9. Giaccone, G., et al., *Phase II study of belinostat in patients with recurrent or refractory advanced thymic epithelial tumors.* J Clin Oncol, 2011. **29**(15): p. 2052-9.
10. Ljubenkov, P.A., et al., *Effect of the Histone Deacetylase Inhibitor FRM-0334 on Progranulin Levels in Patients With Progranulin Gene Haploinsufficiency: A Randomized Clinical Trial.* JAMA Netw Open, 2021. **4**(9): p. e2125584.
11. Lahm, A., et al., *Unraveling the hidden catalytic activity of vertebrate class IIa histone deacetylases.* Proc Natl Acad Sci U S A, 2007. **104**(44): p. 17335-40.
12. Martin, M., R. Kettmann, and F. Dequiedt, *Class IIa histone deacetylases: regulating the regulators.* Oncogene, 2007. **26**(37): p. 5450-67.
13. Das Gupta, K., et al., *Class IIa Histone Deacetylases Drive Toll-like Receptor-Inducible Glycolysis and Macrophage Inflammatory Responses via Pyruvate Kinase M2.* Cell Rep, 2020. **30**(8): p. 2712-2728 e8.
14. Shakespear, M.R., et al., *Histone deacetylase 7 promotes Toll-like receptor 4-dependent proinflammatory gene expression in macrophages.* J Biol Chem, 2013. **288**(35): p. 25362-25374.
15. Guerriero, J.L., et al., *Class IIa HDAC inhibition reduces breast tumours and metastases through anti-tumour macrophages.* Nature, 2017. **543**(7645): p. 428-432.
16. Zhang, W., et al., *Class IIa HDAC inhibitor TMP195 alleviates lipopolysaccharide-induced acute kidney injury.* Am J Physiol Renal Physiol, 2020. **319**(6): p. F1015-F1026.
17. Kopitar-Jerala, N., *Innate Immune Response in Brain, NF-Kappa B Signaling and Cystatins.* Front Mol Neurosci, 2015. **8**: p. 73.
18. Wertz, I.E. and V.M. Dixit, *Signaling to NF-kappaB: regulation by ubiquitination.* Cold Spring Harb Perspect Biol, 2010. **2**(3): p. a003350.
19. Hayden, M.S. and S. Ghosh, *Shared principles in NF-kappaB signaling.* Cell, 2008. **132**(3): p. 344-62.
20. Yu, H., et al., *Targeting NF-kappaB pathway for the therapy of diseases: mechanism and clinical study.* Signal Transduct Target Ther, 2020. **5**(1): p. 209.
21. Luan, B., et al., *Leptin-mediated increases in catecholamine signaling reduce adipose tissue inflammation via activation of macrophage HDAC4.* Cell Metab, 2014. **19**(6): p. 1058-65.
22. Yang, Q., et al., *Histone deacetylase 4 inhibits NF-kappaB activation by facilitating IkappaBalpha sumoylation.* J Mol Cell Biol, 2020. **12**(12): p. 933-945.
23. Asare, Y., et al., *Histone Deacetylase 9 Activates IKK to Regulate Atherosclerotic Plaque Vulnerability.* Circ Res, 2020. **127**(6): p. 811-823.
24. Wallner, M., et al., *HDAC inhibition improves cardiopulmonary function in a feline model of diastolic dysfunction.* Sci Transl Med, 2020. **12**(525).
25. Yang, X., et al., *Transgenic inhibition of astroglial NF-kappaB restrains the neuroinflammatory and neurodegenerative outcomes of experimental mouse glaucoma.* J Neuroinflammation, 2020. **17**(1): p. 252.

26. Lattke, M., et al., *Transient IKK2 activation in astrocytes initiates selective non-cell-autonomous neurodegeneration.* Mol Neurodegener, 2017. **12**(1): p. 16.
27. Chen, Y., et al., *HDAC-mediated deacetylation of NF-kappaB is critical for Schwann cell myelination.* Nat Neurosci, 2011. **14**(4): p. 437-41.
28. Leus, N.G., M.R. Zwinderman, and F.J. Dekker, *Histone deacetylase 3 (HDAC 3) as emerging drug target in NF-kappaB-mediated inflammation.* Curr Opin Chem Biol, 2016. **33**: p. 160-8.
29. Zhang, W.B., et al., *Inhibition of HDAC6 attenuates LPS-induced inflammation in macrophages by regulating oxidative stress and suppressing the TLR4-MAPK/NF-kappaB pathways.* Biomed Pharmacother, 2019. **117**: p. 109166.
30. Xu, C., et al., *Histone deacetylase 5 deacetylates the phosphatase PP2A for positively regulating NF-kappaB signaling.* J Biol Chem, 2021. **297**(6): p. 101380.
31. Li, B., et al., *HDAC5 promotes intestinal sepsis via the Ghrelin/E2F1/NF-kappaB axis.* FASEB J, 2021. **35**(7): p. e21368.
32. Lian, H., et al., *NFkappaB-activated astroglial release of complement C3 compromises neuronal morphology and function associated with Alzheimer's disease.* Neuron, 2015. **85**(1): p. 101-115.
33. Litvinchuk, A., et al., *Complement C3aR Inactivation Attenuates Tau Pathology and Reverses an Immune Network Deregulated in Tauopathy Models and Alzheimer's Disease.* Neuron, 2018. **100**(6): p. 1337-1353 e5.
34. Shi, Q., et al., *Complement C3 deficiency protects against neurodegeneration in aged plaque-rich APP/PS1 mice.* Sci Transl Med, 2017. **9**(392).
35. Hammond, J.W., et al., *Complement-dependent synapse loss and microgliosis in a mouse model of multiple sclerosis.* Brain Behav Immun, 2020. **87**: p. 739-750.

Tables

Table 1 RT-qPCR primers used in the study

Target gene	Forward	Reverse
HDAC4	AGCAGCACCAGCAGTTCCT	CCGCTTCTTCCTCCTCACTCT
HDAC5	AGCAGCACCAGCAGTTCCT	CACTCTCGCCATCCTCATCCT
HDAC7	CGCAGCCAGTGTGAGTGTCT	GCTCGTTCCAGATGGTGTCAGTA
HDAC9	GATGATGATGCCTGTGGTGGAT	TGCTGCTGCTGCTGAATAAGAA
Il-1α	CGCTTGAGTCGGCAAAGAAAT	CTTCCCGTTGCTTGACGTTG
Il-1β	GCAACTGTTCCTGAACTCAACT	ATCTTTTGGGGTCCGTCAACT
Il6	TAGTCCTTCCTACCCCAATTTCC	TTGGTCCTTAGCCACTCCTTC
Tnfα	CCCTCACACTCAGATCATCTTCT	GCTACGACGTGGGCTACAG
C3	AAG CAT CAA CAC ACC CAA CA	CTT GAG CTC CAT TCG TGA CA
Gfap	AGAAAGGTTGAATCGCTGGA	CGGCGATAGTCGTTA
Ptgs2	GTCTGGTGCCTGGTCTGATGATG	TCTGATACTGGAACTGCTGGTTGAA
Nos2	CCCTTCCGAAGTTTCTGGCAGCAGC	GGCTGTCAGAGCCTCGTGGCTTTGG
LCN2	CAGGACTCAACTCAGAACT	GCTCATAGATGGTGCTGTA
β-actin	CCACCATGTACCCAGGCATT	CGGACTCATCGTACTCCTGC

Figures

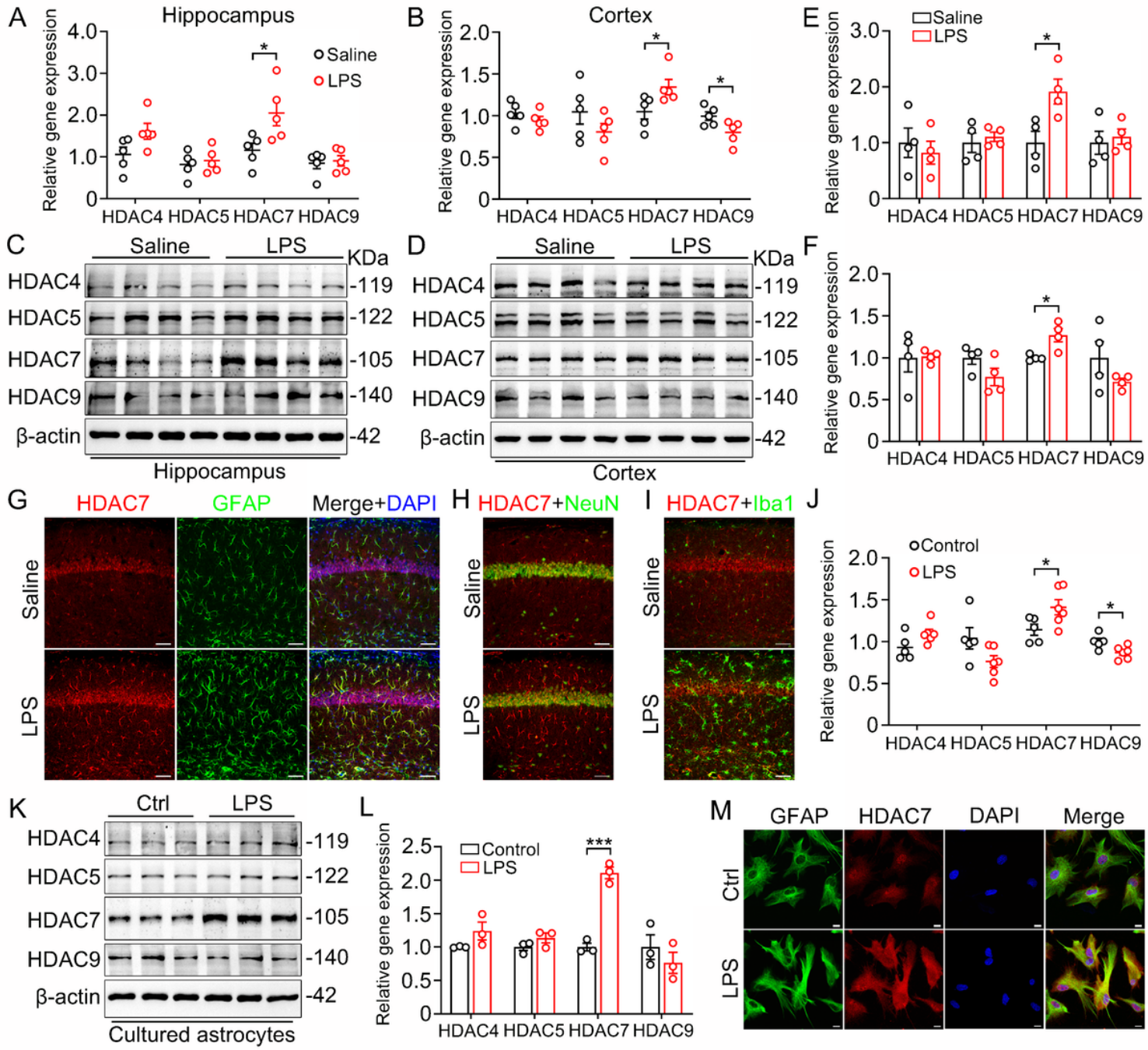

Figure 1

HDAC7 level is selectively increased in LPS-stimulated astrocytes in vivo and in vitro

(A and B) mRNA expression of class IIa HDACs analyzed by RT-qPCR in hippocampus (A) and cortex (B) of LPS- and saline-injected mice (wildtype 2-mon-old C57BL/6 male were intraperitoneally injected with LPS (3mg/kg) or normal saline and sacrificed 24 hours after injection). N = 5 mice for each group, unpaired Student's t test.

(C-F) Representative western blots of HDAC4, HDAC5, HDAC7, HDAC9 and β-actin in hippocampal (C) and cortical (E) lysates of LPS-treated and control mice. Quantification of HDAC4, HDAC5, HDAC7, HDAC9

protein levels in hippocampus (D) and cortex (F), β-actin was used as a loading control. N = 4 mice for each group, unpaired Student's t test.

(G-I) Co-staining of GFAP, NeuN, Iba1 and HDAC7 in the hippocampus after LPS injection. Scale bars, 80 μm.

(J) RT-qPCR analysis of HDAC4, HDAC5, HDAC7, HDAC9 mRNA expression in primary cultured mouse astrocytes after stimulation with LPS (100 ng/ml) for 24 hours. (K) Representative western blots of HDAC4, HDAC5, HDAC7, HDAC9 and β-actin in LPS-treated primary astrocytes. N = 3 for each group, unpaired Student's t test. (L) Quantification analysis of HDAC4, HDAC5, HDAC7, HDAC9 protein levels normalized to β-actin. N = 3 for each group, unpaired Student's t test.

(M) Representative immunofluorescence image of GFAP and HDAC7 co-staining in LPS-treated primary astrocytes.

Data were expressed as mean ± SEM, $*p < 0.05$, $***p < 0.001$.

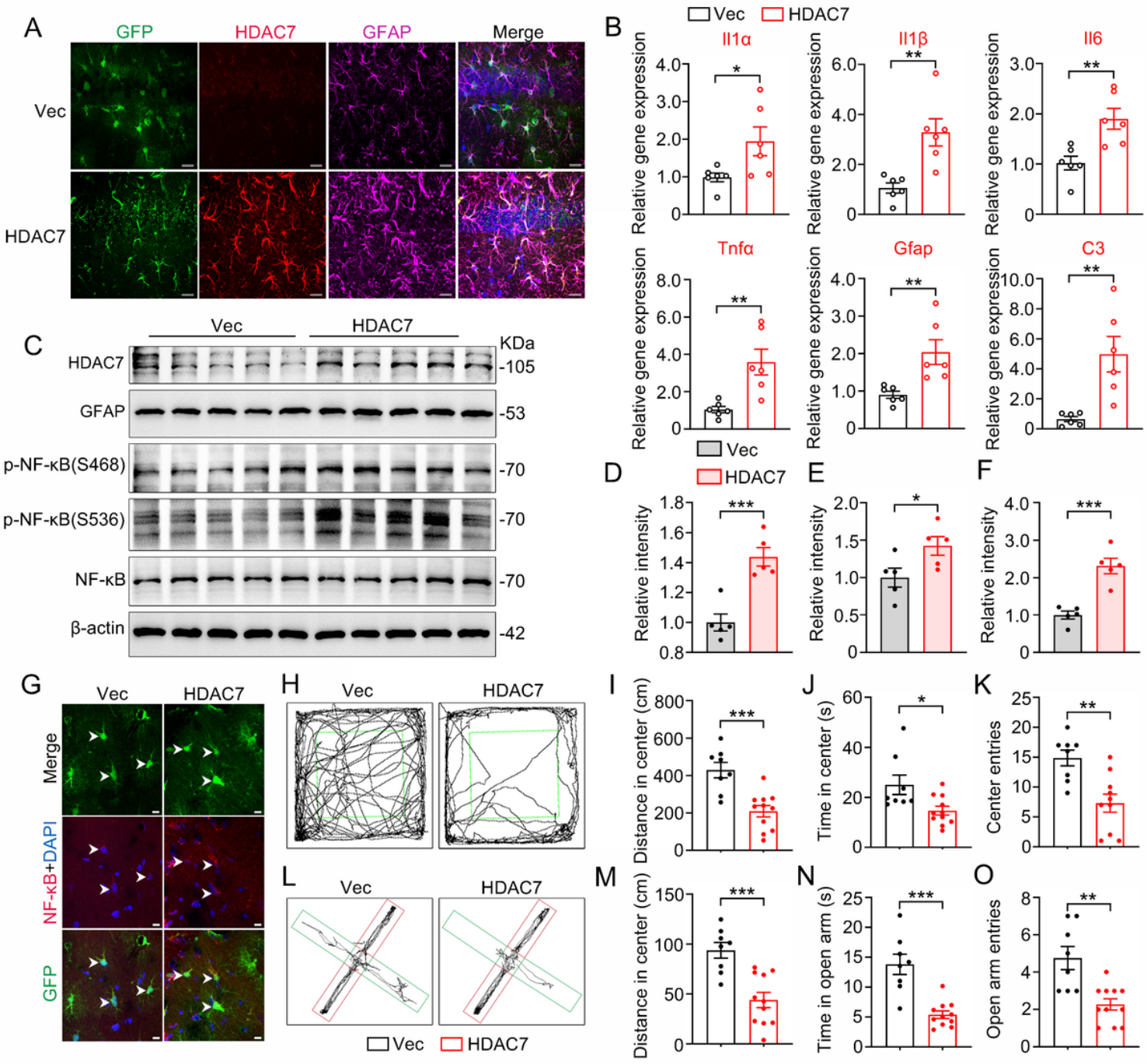

Figure 2

Astrocyte-specific overexpression of HDAC7 leads to neuroinflammation and anxiety-like behaviors in mice

AAV-GfaABC1D-HDAC7-eGFP or the empty vector was stereotaxically infused into the hippocampal CA1 subset of 2-mon-old wildtype mice. After expression for one month, behavioral tests were performed.

(A) Representative confocal image showing the co-expression of GFP, HDAC7 and GFAP in the dorsal hippocampal CA1 subset of 2-mon-old mice. Scale bar, 50 μm.

(B) Astrocytic overexpression of HDAC7 increases mRNA levels of Il-1α, Il-1β, Il6, Tnfα, Gfap and C3 analyzed by RT-qPCR in the hippocampus. N = 6 mice for each group, unpaired Student's t test.

(C-F) Astrocytic overexpression of HDAC7 activates NF-κB activity. (C) Representative western blots of HDAC7, GFAP, p-NF-κB(S468), p-NF-κB(S536), NF-κB and β-actin in the HDAC7-overexpressing and control hippocampal CA1 lysates. Quantification analysis of GFAP protein levels normalized to β-actin (D), p-NF-κB(S468) normalized to total NF-κB (E) and p-NF-κB(S536) normalized to total NF-κB (F). N = 5 mice for each group, unpaired Student's t test.

(G) Representative immunofluorescence image showing enhanced nuclear NF-κB expression in HDAC7-overexpressing and control astrocytes. Scale bar, 10 μm.

(H-K) Overexpression of HDAC7 results in anxiety-like behaviors in the open field test. In this paradigm, the exploring performance in the center region (green frame area) is tested (H). HDAC7-overexpressing mice show decreased center moving distance (I), center exploring time (J) and center entries (K) in the open field test. N = 8-11 mice, unpaired Student's t test.

(L-O) Overexpression of HDAC7 results in anxiety-like behaviors in the elevated plus maze. In this paradigm, the exploring performance in the open arm (green frame area) is tested (L). HDAC7 mice show decreased open arm moving distance (M), open arm exploring time (N) and open arm entries (O) in the elevated plus maze. N = 8-11 mice, unpaired Student's t test.

Data were expressed as mean ± SEM, $*p < 0.05$, $**p < 0.01$, $***p < 0.001$.

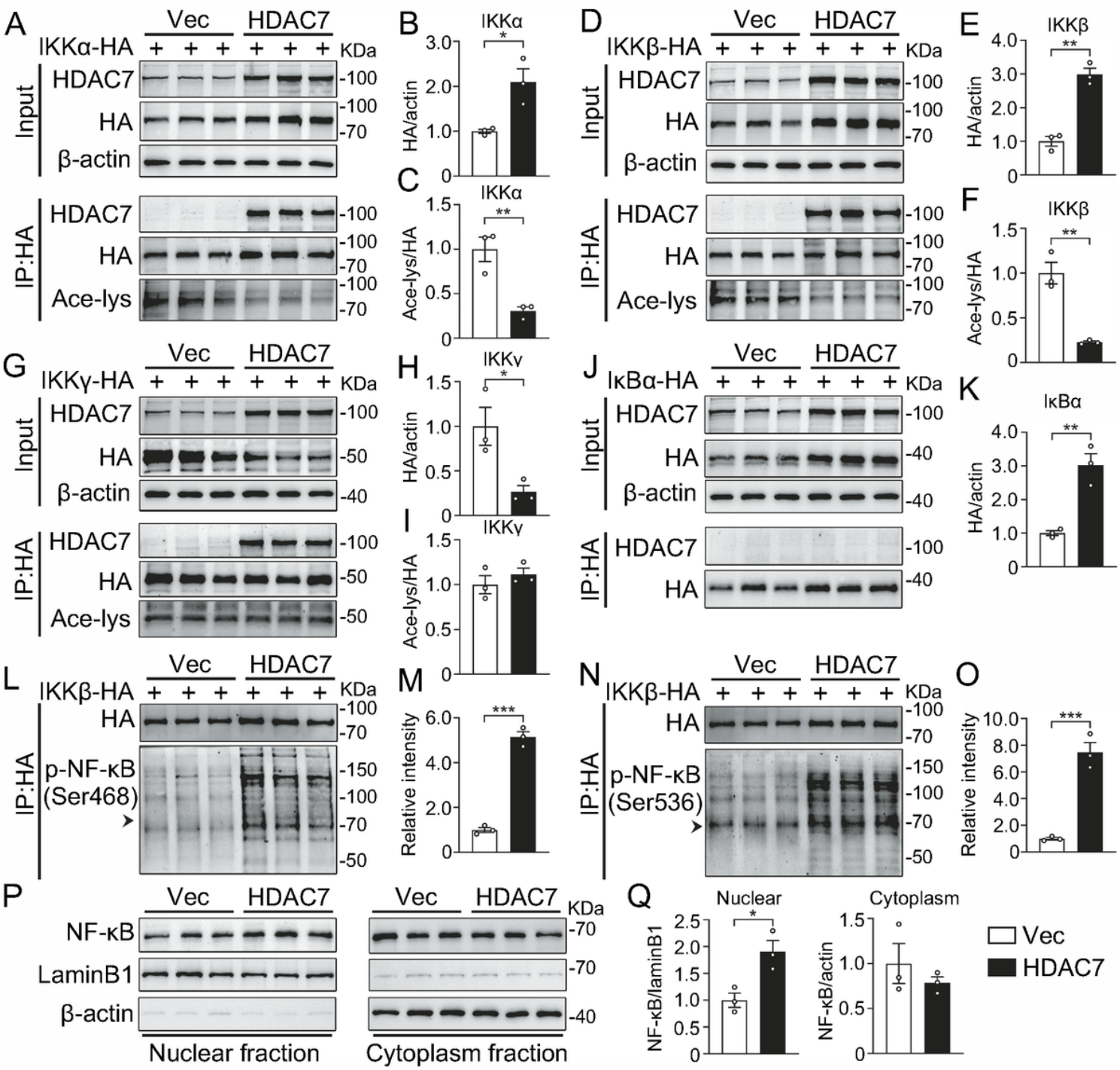

Figure 3

HDAC7 activates IKK through binding to and deacetylating IKKα and IKKβ

HEK293 cells were transiently co-transfected with pcDNA3.1-HDAC7 and individual components of the IKK complex (HA-IKKα, HA-IKKβ, or HA-IKKγ) or HA-IκBα. Co-immunoprecipitation with anti-HA antibodies was performed after transfection for 24 hours.

(A-F) HDAC7 binds to and deacetylates IKKα and IKKβ. Representative immunoblots of HDAC7, HA and Ace-lysine in HA-immunoprecipitated components and input fraction of IKKα+HDAC7 group (A) and

IKKβ+HDAC7 group (D) are shown respectively. Quantification of total IKKα normalized to β-actin (B) and acetylated IKKα normalized to total IKKα (C). Quantification of total IKKβ normalized to β-actin (E) and acetylated IKKβ normalized to total IKKβ (F). N = 3 for each group, unpaired Student's t test.

(G-I) HDAC7 binds to IKKγ with no effects on IKKγ acetylation. (G) Representative immunoblots show expression level of HDAC7, HA and Ace-lysine in HA-immunoprecipitated components and input fraction of IKKγ+HDAC7 and IKKγ+Vec cells. Quantification of total IKKγ normalized to β-actin (H) and acetylated IKKγ normalized to total IKKγ (I). N = 3 for each group, unpaired Student's t test.

(J-K) HDAC7 has no interaction with IκBα. (J) Representative immunoblots show expression level of HDAC7, HA in HA-immunoprecipitated components and input fraction of IκBα+HDAC7 and control cells. (K) Quantification of total IκBα normalized to β-actin. N = 3 for each group, unpaired Student's t test.

(L-O) HDAC7 improves IKK activity showed by increased levels of p-NF-κB(S468) (L) and p-NF-κB(S536) (N) in HA-immunoprecipitated fraction. (M) Quantification analysis of p-NF-κB(S468) normalized to total IKKβ. (O) Quantification analysis of p-NF-κB(S536) normalized to total IKKβ. N = 3 for each group, unpaired Student's t test.

(P and Q) Overexpression of HDAC7 increases NF-κB nuclear localization. (P) Representative immunoblots of NF-κB, LaminB1 and β-actin in nuclear and cytoplasm fraction. (Q) Quantification of nuclear NF-κB normalized to LaminB1 and cytoplasm NF-κB normalized to β-actin. N = 3 for each group, unpaired Student's t test.

Data were expressed as mean ± SEM, $*p < 0.05$, $**p < 0.01$, $***p < 0.001$.

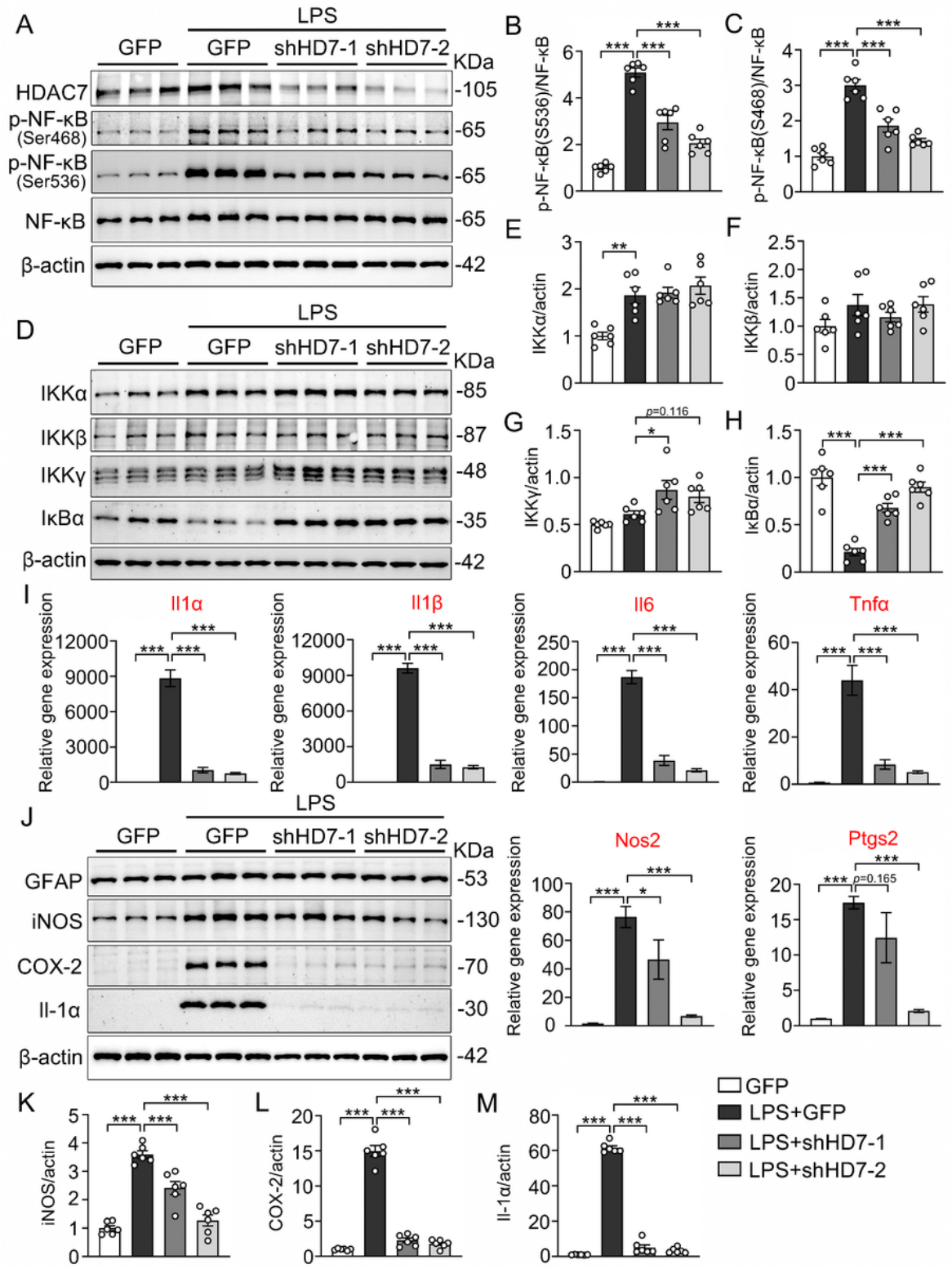

Figure 4

Genetic knockdown of HDAC7 suppresses LPS-induced NF-κB activation and inflammatory responses in primary cultured astrocytes

(A-C) Knockdown of HDAC7 inhibits LPS-induced NF-κB activation in cultured astrocytes. (A) Representative western blots showing protein levels of HDAC7, p-NF-κB(S468), p-NF-κB(S536), NF-κB and

β-actin in control and LPS-treated primary cultured mouse astrocytes (astrocytes were infected with Lenti-GfaABC1D-HDAC7-T2A-GFP or Lenti-GfaABC1D-T2A-GFP for 5 days, and then treated with LPS (100ng/ml) for 24 hours). (B) Quantification analysis of p-NF-κB(S468) normalized to total NF-κB. (C) Quantification analysis of p-NF-κB(S536) normalized to total NF-κB. N = 6 for each group, one-way ANOVA, Dunnett's post hoc analysis.

(D-H) Knockdown of HDAC7 suppresses IκBα degradation with little effects on IKK expression. (D) Representative western blots showing protein levels of IKKα, IKKβ, IKKγ, IκBα and β-actin in control and LPS-stimulated primary mouse astrocytes as described above. (E-H) Quantification of IKKα (E), IKKβ (F), IKKγ (G), IκBα (H) normalized to β-actin. N = 6 for each group, one-way ANOVA, Dunnett's post hoc analysis.

(I-M) Knockdown of HDAC7 inhibits LPS-induced inflammatory responses in cultured astrocytes. (I) RT-qPCR analysis of Il-1α, Il-1β, Il6, Tnfα, INOS and Ptgs2 in control and LPS-stimulated primary cultured mouse astrocytes as described above. (J) Representative western blots showing protein levels of GFAP, INOS, COX-2, Il-1α and β-actin in control and LPS-treated primary cultured mouse astrocytes. (K-M) Quantification of INOS (K), COX-2 (L) and Il-1α (M) normalized to β-actin. N = 6 for each group, one-way ANOVA, Dunnett's post hoc analysis.

Data were expressed as mean ± SEM, $*p < 0.05$, $**p < 0.01$, $***p < 0.001$.

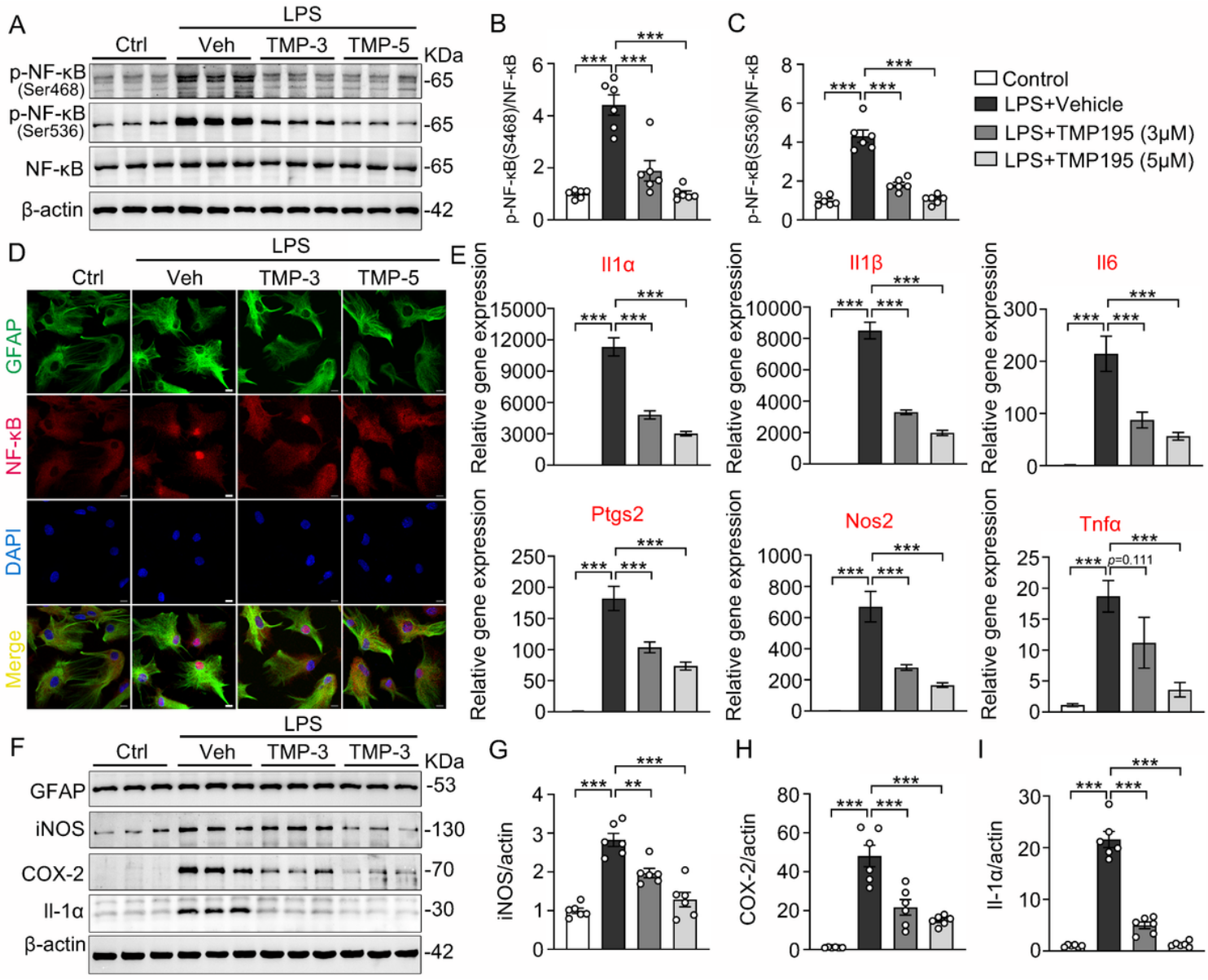

Figure 5

Pharmacological inhibition of HDAC7 with TMP195 suppresses LPS-induced NF-κB activation and inflammatory responses in primary cultured astrocytes

(A-C) TMP195 blocks LPS-induced NF-κB phosphorylation in cultured astrocytes. (A) Representative western blots showing protein levels of p-NF-κB(S468), p-NF-κB(S536), NF-κB and β-actin in LPS- and TMP195-treated primary cultured mouse astrocytes (astrocytes were incubated with LPS (100ng/ml), LPS (100ng/ml) + TMP195 (3μM), LPS (100ng/ml) + TMP195 (5μM) or control vehicle for 24 hours). (B) Quantification of p-NF-κB(S468) normalized to total NF-κB. (C) Quantification of p-NF-κB(S536) normalized to total NF-κB. N = 6 for each group, one-way ANOVA, Dunnett's post hoc analysis.

(D) Representative confocal image showing decreased nuclear NF-κB expression by TMP195 in LPS-stimulated astrocytes described as above. Scale bar, 10 μm. N = 6 for each group, one-way ANOVA, Dunnett's post hoc analysis.

(E-I) TMP195 reverses LPS-induced inflammatory responses in cultured astrocytes. (E) RT-qPCR analysis of Il-1α, Il-1β, Il6, Tnfα, INOS and Ptgs2 in LPS and TMP195- treated astrocytes described as above astrocytes described as above. (F) Representative western blots showing protein levels of GFAP, INOS, COX-2, Il-1α and β-actin in primary astrocytes treated as described above. (G-I) Quantification of INOS (G), COX-2 (H) and Il-1α (I) normalized to β-actin. N = 6 for each group, one-way ANOVA, Dunnett's post hoc analysis.

Data were expressed as mean ± SEM, $**p < 0.01$, $***p < 0.001$.

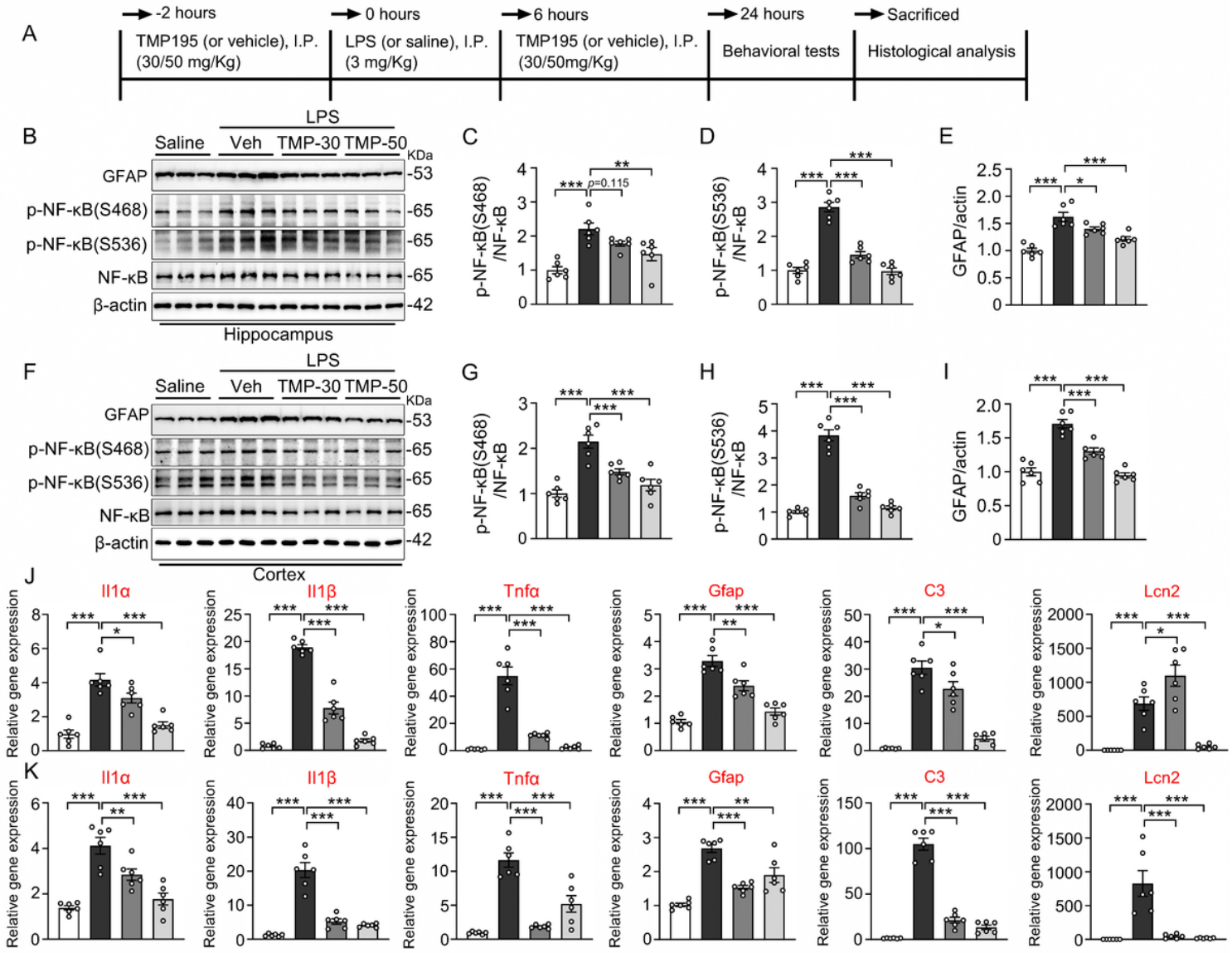

Figure 6

TMP195 decreases LPS-induced NF-κB activation and neuroinflammation in vivo

(A) Schematic diagram of the experimental procedure in mice. 2-mon-old wildtype C57BL/6 male mice were pre-injected with TMP195 (30/50mg/kg) or vehicle 2 hours before LPS (3mg/kg) injection and received another injection of TMP195 (30/50mg/kg) 6 hours after LPS treatment.

(B-I) TMP195 attenuates LPS-induced NF-κB activation in vivo. (B) Representative western blots showing protein levels of GFAP, p-NF-κB(S468), p-NF-κB(S536), NF-κB and β-actin in hippocampus. (C-E) Quantification of p-NF-κB(S468) normalized to total NF-κB (C), p-NF-κB(S536) normalized to total NF-κB (D), GFAP normalized to β-actin (E) in hippocampus. (F) Representative western blots showing protein levels of GFAP, p-NF-κB(S468), p-NF-κB(S536), NF-κB and β-actin in coxtex. (G-I) Quantification of p-NF-κB(S468) normalized to total NF-κB (G), p-NF-κB(S536) normalized to total NF-κB (H), GFAP normalized to β-actin (I) in cortex. N = 6 for each group, one-way ANOVA, Dunnett's post hoc analysis.

(J and K) TMP195 reverses LPS-induced inflammatory gene expression in vivo. (J) RT-qPCR analysis of Il-1α, Il-1β, Tnfα, Gfap, C3 and Lcn2 gene expression in hippocampus. (K) RT-qPCR analysis of Il-1α, Il-1β, Tnfα, Gfap, C3 and Lcn2 gene expression in cortex. N = 6 for each group, one-way ANOVA, Dunnett's post hoc analysis.

Data were expressed as mean ± SEM, $*p < 0.05$, $**p < 0.01$, $***p < 0.001$.

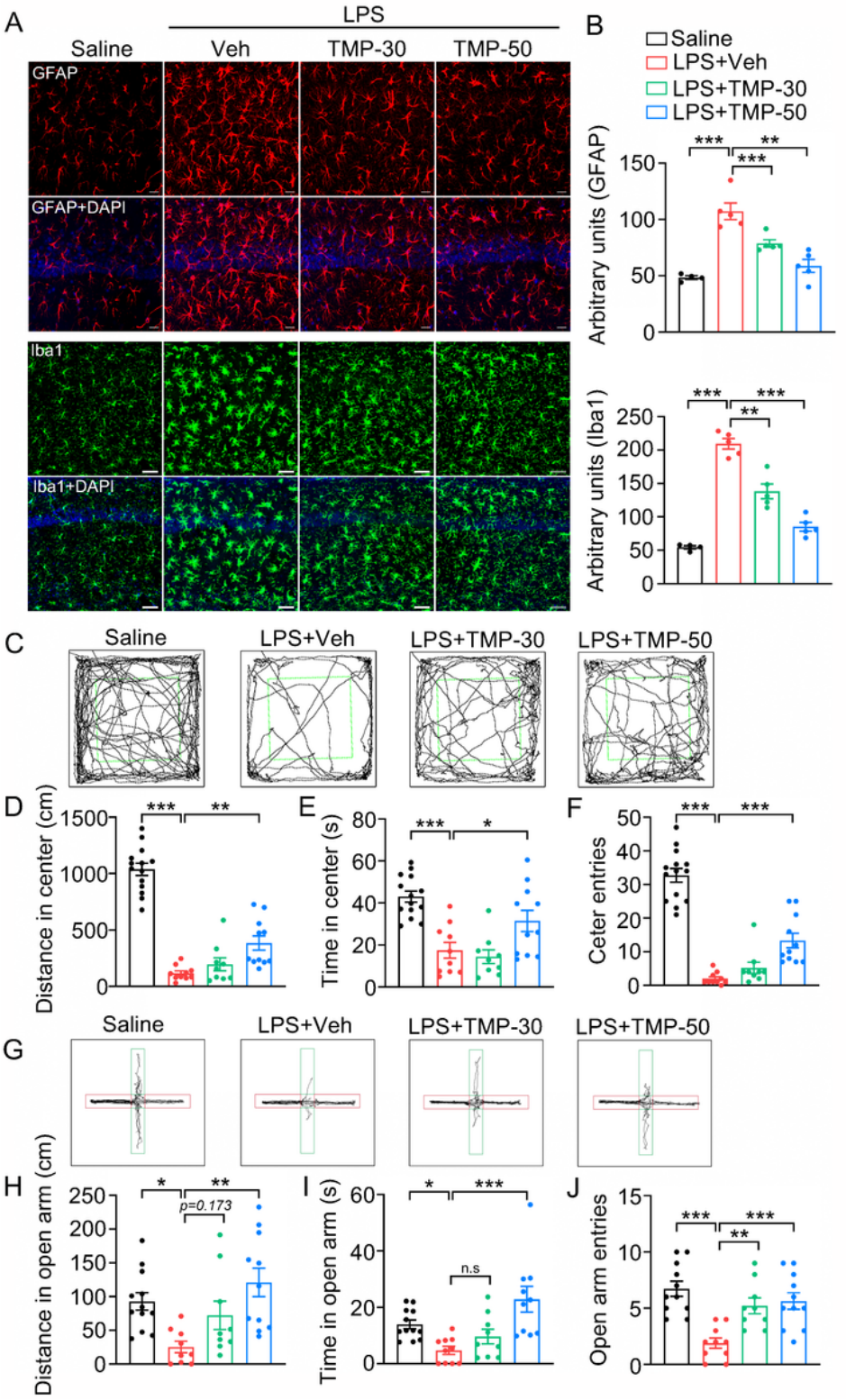

Figure 7

TMP195 reverses LPS-induced gliosis and anxiety-like disorders in vivo

(A and B) TMP195 limits LPS-induced gliosis. (A) Representative confocal image of GFAP and Iba1 in the hippocampal CA1 subset. (B) Quantification of GFAP and Iba1 immunofluorescence intensity in the hippocampus. N = 4-5 for each group, one-way ANOVA, Dunnett's post hoc analysis.

(C-F) TMP195 attenuates LPS-induced anxiety-like disorders in the open field test. In this test, the exploring performance in the center region (green frame area) is tested. (C) Representative moving traces of mice during the open field test. TMP195 treatment attenuates LPS-induced exploring disorders represented by increased center moving distance (D), center exploring time (E) and center entries (F) in the open field test. N = 9-14 mice, one-way ANOVA, Dunnett's post hoc analysis.

(G-J) TMP195 ameliorates LPS-induced anxiety-like disorders in the elevated plus maze. (G) Representative moving traces of mice during the elevated plus maze. TMP195 treatment improved exploring capacity of LPS-injected mice shown by increased open arm moving distance (H), open arm exploring time (I) and open arm entries (J) in the elevated plus maze. N = 9-14 mice, one-way ANOVA, Dunnett's post hoc analysis.

Data were expressed as mean ± SEM, $*p < 0.05$, $**p < 0.01$, $***p < 0.001$.

Supplementary Files

This is a list of supplementary files associated with this preprint. Click to download.

- supplementary.docx